Acta Montanistica Slovaca
ISSN 1335-1788
actamont.tuke.sk

A Comparative Study of Anionic and Cationic Collector in Microbubble-Assisted Flotation for Coarse Quartz Particle: Performance and Adsorption

Ahmed ABBAKER[1,3]* *and* *Nevzat ASLAN*[2]

Authors' affiliations and addresses:
[1] FEN Bilimleri Enstitüsü, Sivas Cumhuriyet University, 58140 Sivas, Türkiye
e-mail: 20199223001@cumhuriyet.edu.tr

[2] Industrial Engineering Department, Sivas Cumhuriyet University, 58140 Sivas, Türkiye
e-mail: naslan@cumhuriyet.edu.tr

[3] Department of Mining Engineering, Faculty of Engineering Sciences, Omdurman Islamic University, P.O.BOX Khartoum 10257, Omdurman 382, Sudan
e-mail: a7medelmubarak@oiu.edu.sd,

***Correspondence:**
Ahmed ABBAKER, Department of Mining Engineering, Faculty of Engineering Sciences, Omdurman Islamic University, P.O.BOX Khartoum 10257, Omdurman 382, Sudan
tel.: +905342004977
e-mail: a7medelmubarak@oiu.edu.sd

How to cite this article:
Abbaker, A. and Aslan, N. (2024). A Comparative Study of Anionic and Cationic Collector in Microbubble-Assisted Flotation for Coarse Quartz Particle: Performance and Adsorption. *Acta Monstanistica Slovaca,* Volume 29 (2), 239-255

DOI:
https://doi.org/10.46544/AMS.v29i2.01

Abstract
Recent studies have suggested that using microbubbles to assist in coarse particle flotation has some advantages. However, how the type of collector affects the recovery of coarse particles under microbubbles still needs to be clarified. This study compared the performance and adsorption characteristics of anionic (sodium oleate - NaOL) and cationic (dodecylamine - DDA) collector environments for microbubble-assisted flotation of coarse quartz particles. A two-factorial level and Box-Behnken techniques were used for statistical design for screening and characterizing the performance. The flotation process utilizing NaOL and DDA was not significantly affected by froth depth. In the presence and absence of microbubbles, the performance of DDA surpassed that of NaOL; therefore, the average recovery of the cationic collector was more than 10% higher than that of the anionic collector. Contact angle analysis revealed that NaOL measured approximately 70° while DDA measured around 90°. DDA was adsorbed more significantly than NaOL at the same collector concentration. Zeta potential was more sensitive to DDA; increasing both collector concentrations also increased the value of zeta potential. FT-IR and EDX analyses showed that DDA and NaOL were chemically adsorbed onto quartz. Overall, this study demonstrates that DDA outperformed NaOL in the presence and absence of microbubbles during the flotation of coarse quartz particles.

Keywords
Coarse Particle, Microbubbles, Adsorption, Dodecylamine, Sodium Oleate, Statistical Analysis.

Introduction

Every separation has used the distinctions in characteristics between gangue and valuable minerals. Froth flotation builds on variations in a mineral's surface characteristics that might occur naturally or through manipulation. Many different things affect the flotation process, such as the ionic properties of the medium, the interfacial properties of solids, hydrodynamics, energetics, kinetics, and the properties of the reagents and gases (Elvers, 1991; Rao, 2013). Collectors are significant in flotation because they change the adsorption chemistry and strength. The choice between anionic and cationic collectors in flotation depends on the ore's specific mineralogical composition and the target minerals' surface charge characteristics. It involves a balance between achieving high selectivity and economic considerations. The mechanism of reagent adsorption on mineral surfaces has been thoroughly investigated in the past several years, and analytical instruments, including zeta potential, FT-IR, and contact angle, are frequently employed. Minerals can adsorb substances because they have hydroxyl groups on their surfaces that participate in the dissociative chemisorption of the adsorbate. Numerous variables affect mineral surface protonation and reagent adsorption, such as reagent concentration, pH, and particle size (Fu et al., 2022).

The flotation process requires a certain size range of particles, ranging from 10 to 150 μm, based on their density (Duffy et al., 2013). The flotation process is a costly technique in mineral processing due to the necessity for expensive pulverization of a tiny size range and the required chemical reagents (Farrokhpay et al., 2021). The simple flotation process consists of a collision between particles and air bubbles, resulting in their colloidal, and finally, this colloidal of a bubble-particle securely moves to the froth phase (Darabi et al., 2019). Poor coarse particle flotation recovery is mainly caused by a strong detachment and weak attachment efficiencies (Abbaker & Nevzat, 2023; Carlos et al., 2007; Darabi et al., 2019; Rahman et al., 2012; Tao, 2005). There have been suggestions that additional factors are the reasons for coarse particle flotation difficulties. For example, the high density of large particles has been linked to poor suspension, which causes the particles to be at the bottom of the cell without enough turbulence, decreasing the chance of a particle being collected (Ata & Jameson, 2013; Duffy et al., 2013; Jameson, 2010). The presence of strong turbulence inside the conventional cell directly impacts the stability of the bubble-particle aggregate, increasing the likelihood of particle detachment (Ata & Jameson, 2013; Carlos et al., 2007; Duffy et al., 2013; Farrokhpay et al., 2011; Jameson, 2010; Rahman et al., 2012; Tao, 2005; Xu et al., 2011). Mechanically agitated flotation machines are the most often used in the mining sector. It is scarce for mining and mineral processing to use coarse flotation techniques, even though most work better than standard cells (Hassanzadeh et al., 2022; Nazari et al., 2022). This scarcity is because making and testing new flotation cell designs is very expensive and dangerous. Also, the current methods for separating coarse particles, like fluidized-bed flotation cells, have some problems. For example, they have low surface energy, poor recovery, trouble getting rid of fine particles, slow flotation rates, and particles coming off (Kromah et al., 2022).

Microbubbles adhere to particles more efficiently than ordinary bubbles because of their greater surface area and lower rising velocity. Large bubbles prefer to adhere to microbubbles more than particles., so combining microbubbles and large bubbles leads to enhanced flotation recovery of coarse particles. Microbubbles function as an additional particle collector, reducing the amount of flotation collector required, enhancing the attachment, and diminishing the detachment (Nazari et al., 2019; Nazari & Hassanzadeh, 2020; Tao, 2005). For fine and ultrafine particles, a similar technique of blending microbubbles with coarse bubbles has been used with success (Farrokhpay et al., 2020; Rulyov et al., 2018, 2021; Tussupbayev et al., 2016).

Expanding the limit size of the particles in the flotation process will decrease the amount of power consumption in the size reduction operation and the quantity of fines generated. Drying, thickening, and filtering are some of the more affordable and accessible processes that follow. Assuming that flotation technology was accessible, it would be determined by the kind of ore. In such situations, there is a potential for raising the maximum grinding size to 500 μm, separating a significant amount of the material in a preliminary coarse process, and then grinding the coarse concentrate to a final size that is suitable for the ore's liberation degree (Jameson, 2010; Tao, 2005).

To fully grasp the performance of the flotation process, it is essential to have a thorough knowledge of the adsorption properties. Several endeavors have been documented to comprehend and enhance the flotation process of large particles. The most recent work was conducted by Nazari and others using microbubbles in a coarse particle flotation system, and the result was promising. Nevertheless, insufficient testing of some variables and disregard for other crucial components have necessitated a more profound comprehension. The use of various collectors will impact the flotation process for larger particles. The hydrodynamic conditions required for the flotation of larger particles vary greatly from those of fine particles (Fosu et al., 2015). Also, the effect of different factors interacting with each other on the flotation process of large particles needs to be considered, mainly when different collectors are used with microbubbles.

The goal of this research is to completely comprehend the effectiveness of cationic and anionic collectors in separating coarse quartz particles, as well as how microbubbles alter the performance of the effective parameters in a mechanical flotation cell using two-factorial level and Box-Behnken statistical analysis.

Materials and Methods

Sample and reagents

The quartz sample is 98% pure and was taken from Kaltun Madencilik - Turkey. According to the Malvern Matersizer's particle size measurement of the typical sample, D50 = 276µm. A sieve was used to eliminate any sample size less than 212µm, as this work focuses on coarse size. Fig. 1 illustrates that D50 = 495µm was obtained by reapplying the particle size measurement. For the investigation, 10 kg of the material was also ground up into tiny particles, the size of which was determined by measurement to be D50 = 40µm. The Pashley and Kitchener technique has been used to clean quartz. After two hours of washing the sample three times with concentrated hydrochloric acid (HCl 37%), the sample was cleaned four times with distilled water. After that, the sample was submerged for a minute at 60 °C in 30% sodium hydroxide (NaOH). Finally, the quartz sample was subjected to overnight drying at a temperature of 110 °C. Two types of spectrometers—X-ray fluorescence (XRF) and X-ray diffraction (XRD)—were used to look at the quartz particles chemically and mineralogically, as shown in Tab. 1 and Fig. 2. MERCK's dodecylamine (DDA) was used as the cationic collector. Moreover, sodium oleate produced by Oxford is used as the anionic collector.

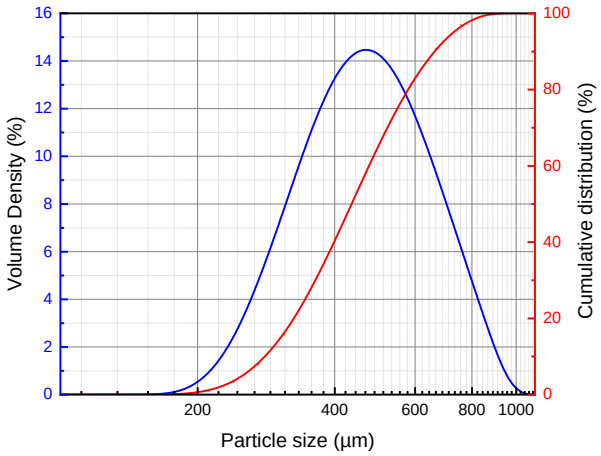

Fig. 1. The quartz sample's size dispersion.

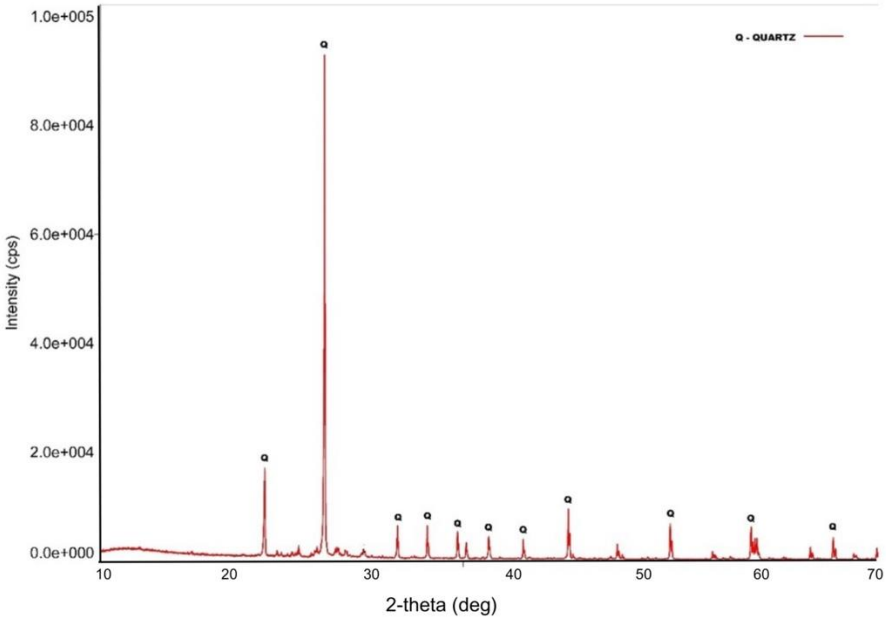

Fig. 2. XRD pattern of quartz.

Table 1. XRF analysis.

Component	SiO_2	Fe_2O_3	P_2O_5	Na_2O	MnO	TiO_2	K_2O	MgO	Al_2O_3	A.Za	CaO
(wt.%)	97.7	0.4	<0.1	0.3	<0.1	<0.1	<0.1	0.1	0.6	0.3	0.2

Microbubbles generator

Only a few technically feasible techniques for producing micro- and nanobubbles—such as electrolysis, water-solvent mixtures, ultrasonic, temperature modulation, and pressure reduction—have been used for flotation systems. It is made up of CMP (two-phase centrifugal multiphase pump), HC (hydrodynamic cavitation), DAF (dissolved air flotation), and MicroGas (MG) (Nazari & Hassanzadeh, 2020). Fig. 3 displays a microbubble generator from China's Dongguan Technology Co. Ltd. A direct-connected motor construction makes up the gas-liquid mixing pump's body. An air compressor and atmospheric ejector are not required since the gas-liquid mixing pump's suction port employs negative pressure to draw gas. The gas and liquid are entirely dissolved because of the pressured mixing in the pump. Therefore, a massive, pressurized gas tank or pricey reaction tower is unnecessary to manufacture a highly dissolved liquid. The centrifugal pump employs a gas-liquid ratio of 1:9 and a flow rate of 20 L/min to produce microbubbles. The resulting microbubbles are between 20 and 30 μm in size.

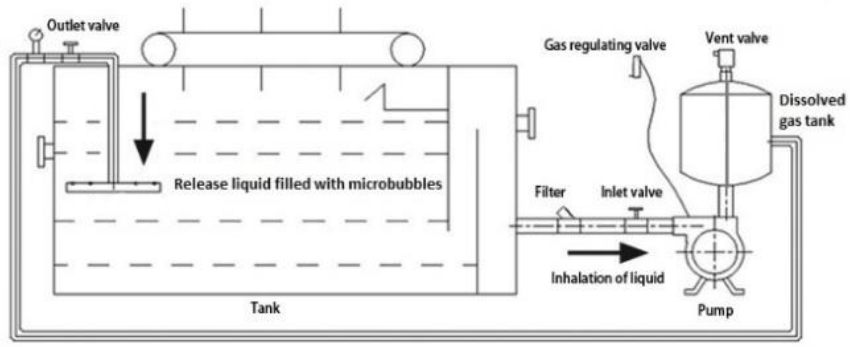

Fig. 3. Microbubbles generator.

Flotation experiment

The present study employed a Denver flotation machine (self-aerated) of model D12 for the investigation. In a 1.2 L cell, the flotation time at room temperature was 4 minutes. Girgin (2006) reported that a self-aerated Denver laboratory apparatus produced giant bubbles when the impeller speed was increased, signifying a rise in air flow rate (Girgin et al., 2006). The pH of the tap water used in the trials was 7.74. The factors that significantly affect the result will be examined for every step, and the ones with little to no effect must be removed. Through a primary focus on dubious or ambiguous components, the screening process aimed to identify the elements that substantially influence recovery. The impacts of these elements were then the main focus of the flotation performance experiments.

Anionic collector

Abbaker and Nevzat (2023) used the following parameters in screening and characterization experiments: pH 12, impeller speed of 950 rpm, and sodium oleate concentration of 2.75 mmol/L. The objective was to ascertain the significant process parameters from unreliable or questionable data, as shown in Tab. 2.

Table 2. Anionic Two-level factor design.

Factors	Explanation	Levels
A	MIBC (mmol/L)	0.1 - 1
B	Pulp concentration (%)	10 - 40
C	Fine particles (%)	0 - 20
D	Froth depth (cm)	1 - 2
E	Calcium oxide (mmol/L)	0.5 - 5

They examined the performance of NaOL on coarse particles by using the Box- Behnken method with a seven-factor design, as presented in Tab. 3.

Table 3. Anionic Box-Behnken response surface design.

Factors	Explanation	Levels
A	MIBC (mmol/L)	0.1 – 1
B	Pulp concentration (%)	10 – 40
C	Fine particles (%)	0 – 20
D	Impeller speed (rpm)	700 – 1200
E	Sodium oleate (mmol/L)	0.5 – 5
F	Calcium oxide (mmol/L)	0.5 - 5
G	Microbubbles	Absent - Present

Cationic collector

Screening tests were conducted in the cationic collector under the following conditions: DDA of 0.1 mmol/L, pH of 8.5, and impeller speed of 950 rpm, which were used to separate important parameters from questionable or unknown ones. A series of flotation experiments (consisting of 20 runs) were carried out using a two-level factorial design, including five points at the center. The purpose was to examine the impact and interplay of MIBC, pulp concentration, fine particles, and froth depth. The operational ranges for these variables were determined based on previous research, as indicated in Tab. 4.

Table 4. Cationic Two-level factor design.

Factors	Explanation	Levels
A	MIBC (mmol/L)	0.1 – 1
B	Pulp concentration (%)	10 – 40
C	Fine particles (%)	0 – 20
D	Froth depth (cm)	1 - 2

The Box-Behnken experimental design with six factors was used to examine how DDA affected coarse particles' flotation over 92 runs. There are five number elements and one category element. The investigations that were carried out to ascertain the effects of fine particles, microbubbles, pulp content, impeller speed, and DDA are displayed in Tab. 5.

Table 5. Cationic Box-Behnken response surface design.

Factors	Explanation	Levels
A	MIBC (mmol/L)	0.1 - 1
B	Pulp concentration (%)	10 - 40
C	Fine particles (%)	0 - 20
D	Impeller speed (rpm)	700 - 1200
E	DDA (mmol/L)	0.1 - 1
F	Microbubbles	Absent - Present

Randomization was used in all performance investigations to minimize bias and neutralize the impact of unanticipated response changes. Analysis of the recoveries and evaluation of the interactions between the process components were conducted using an analysis of variance (ANOVA).

Contact angle measurement and EDX spectroscopy analysis

Pure quartz was also employed to determine the contact angle for the flotation experiments. For treated quartz sample preparation, a quantity of 50 grams from the rough sample was deposited into a beaker with a capacity of 500 mL. Then, the required reagents for a specific method, either anionic or cationic, were added to the beaker. The pulp was agitated for 20 minutes. Subsequently, these treated samples were subjected to filtration, followed by three rounds of washing with distilled water, and finally dried in the oven. Afterward, the examined substances were compressed into tablets, and their contact angle was measured thrice on the NRL. C.A. GONIOMETER (RAME-HART, U.S.A). Moreover, EDX chemical analysis was performed on the dried sample to study the elements on the quartz surface in the pure form after being treated with CaO + NaOL and DDA.

Adsorption capacity experiments

To calculate the quantity of NaOL and DDA adsorbed onto the surface of quartz, the calibration curve method (based on Beer-Lambert law) using ultraviolet spectrophotometry (UV-Vis) was conducted. To find an unknown concentration, known concentrations of collectors were taken, and their absorbance at a fixed wavelength was

measured. Then, a plot of the absorbance and concentration data was fitted with a straight-line equation at a high value of R^2, as shown in the standard curves (Fig. 4). From the equation, unknown concentrations could be calculated from their absorbance values. The method of conducting the solutions was the same as in contact angle measurement, only here, the solutions were collected rather than quartz minerals. The quantity of adsorbed NaOL and DDA was calculated by the Gibbs adsorption formula, Eq. (1):

$$n_{\text{ads}} = \frac{(C_0 - C_{eq})V}{m} \tag{1}$$

where n_{ads} refers to the amount of collector that is adsorbed per gram of quartz (mol/g), C_0 represents the starting concentration of the collector (mol/L), C_{eq} represents the amount of the collector after it went through adsorption. (mol/L), V represents the volume of the solution (L), and m refers to the weight of the quartz sample (g) (Liu et al., 2020).

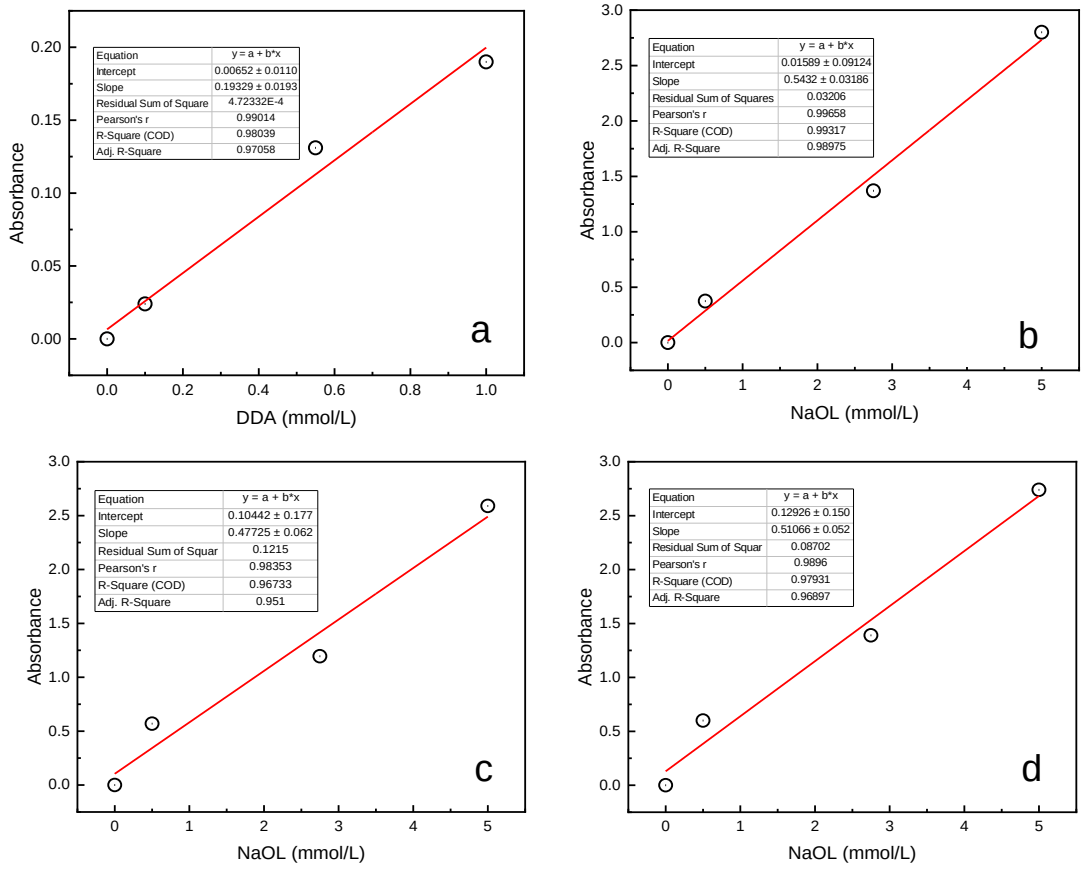

Fig. 4. The standard curve of a) DDA, b) NaOL at $5x10^{-4}$ mol/L of CaO, c) NaOL at $2.75x10^{-3}$ mol/L of CaO, d) NaOL at $5x10^{-3}$ mol/L of CaO.

Zeta potential measurement

A sample of pure quartz was first ground into a very fine size, approximately 10 μm. For each collector and activation concentration, 0.1g of the grounded sample was added to a 100-ml beaker containing 50 ml of 1 x 10^{-3} M KCl. After 2 min of agitation, the pH value was adjusted using 0.01, 0.1, and 0.25 mol of HCl and NaOH to the target, and then the activation (in NaOL case only) and collector were added. After 5 min stirring, the zeta potentials were determined using a Malvern Zetasizer Nano ZS90 with a rectangular electrophoresis cell. The average of three measurements was recorded, and the experiments were maintained at room temperature.

FT-IR spectroscopy analysis

The FT-IR spectra of NaOL, CaO, DDA, and quartz samples before and after interacting with the reagents were performed using a TENSOR II FT-IR Spectrometer (USA) to analyze the chemical functional groups on the quartz particle's surfaces. Samples were prepared by agitating quartz particles less than 15 μm in solutions with different reagent schemes. Firstly, 10g of samples were placed into 100 mL of distilled water, and then the pH of the pulp was modified to either 12 or 8.5, depending on the collector type. Secondly, the specific reagents and

their dosages were added to the pulp and conditioned for 10 min. Third, the solutions were filtered, washed, and dried in a vacuum oven. Finally, the measurements were conducted using KBr pellets at room temperature in the 400 – 4000 cm^{-1} range.

Adsorption chemistry

Throughout the flotation of minerals with DDA, amine molecules and amine ions coexisted in the slurry solution, although their quantities changed, and the pH of the solution fluctuated significantly. A large portion of the solution at high alkalinity consisted of amine molecules, which were far less soluble than amine ions. The system's surface activity reduced, the repulsive force between hydrophilic groups increased, and the H^+ concentration expanded with a high acidity, where the system's surface energy increased. As a result, the DDA performed better in weak acid or weak base conditions, consistent with Fig. 5's findings—the dissolution of DDA at a pH value of 8.5.

$$RNH_2 + H_2O \rightleftharpoons RNH_3^+ + OH^- \quad (2)$$

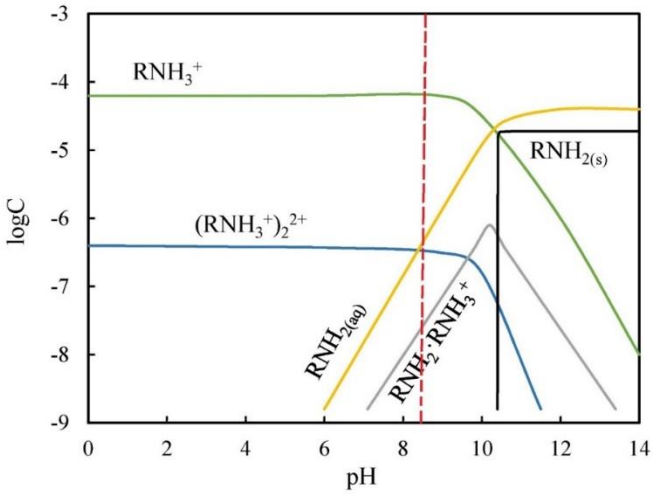

Fig. 5. Species distribution diagram of DDA as a function of pH.

Quartz has a limited float over the pH range in the presence of an anionic collector. However, its floatability significantly improves upon activation with lime (CaO). Figure 6(a) shows that the concentrations of calcium species in a solution depend on its pH. These species are hydroxyl calcium ($Ca(OH)^+$), soluble calcium hydroxide ($Ca(OH)_2(aq)$), and calcium ions (Ca^{2+}) (Cao et al., 2022). Calcium oxide (CaO) dissolution may be mathematically represented by equations (3-6). The pH and concentration influence the presence of calcium ions in solutions.

$$CaO + H_2O \rightarrow Ca(OH)_2 \quad (3)$$

$$Ca(OH)_{2(aq)} \rightleftharpoons Ca(OH)^+ + OH^- \quad (4)$$

$$Ca(OH)^+ \rightleftharpoons Ca^{2+} + OH^- \quad (5)$$

$$Ca(OH)_{2(aq)} \rightleftharpoons Ca^{2+} + 2(OH)^- \quad (6)$$

According to many sources, SiO-Ca(OH) is formed by the adsorption of $Ca(OH)^+$ onto the quartz surfaces of negative charge. Chemisorption refers to the adsorption of oleate ions (Fig. 6(b)) on the activated quartz surface since it involves the formation of covalent bonds. The adsorption may be elucidated using the conventional electron donor/electron acceptor hypothesis, where calcium acts as the electron acceptor, and the oxygen in the $RCOO^-$ functional group serves as the electron donor. Equations (7) and (8) demonstrate the relationship between the oleate ions and the SiO-Ca(OH) on the surface of quartz (Fan et al., 2020). To illustrate the adsorption mechanism further, Fig. 7 presents the origin of charge on quartz when using anionic and cationic collectors.

$$SiO– Ca(OH) + RCOO^- \rightarrow SiOCaOOCR + OH^- \quad (7)$$

$$2SiO– Ca(OH) + (RCOO)^{-2}{}_2 \rightarrow 2SiOCaOOCR + 2OH^- \quad (8)$$

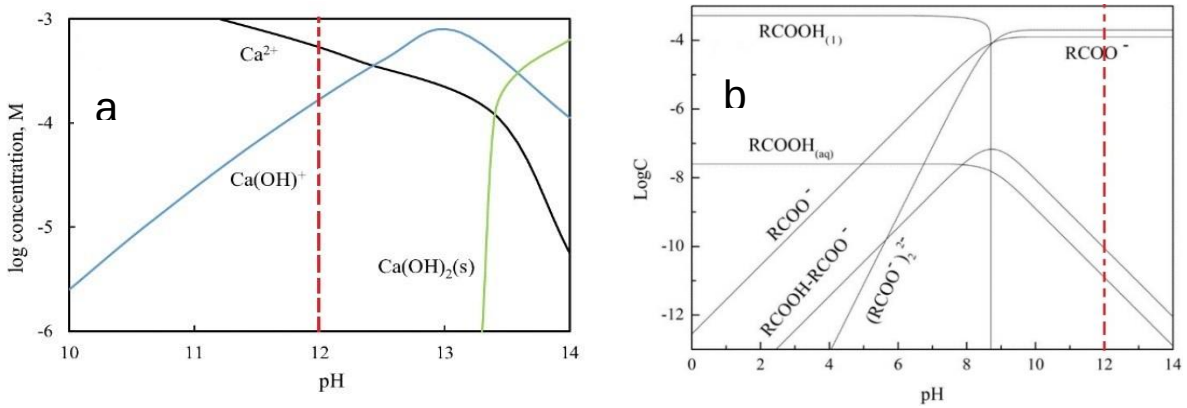

Fig. 6. Species distribution diagram of a) CaO and b) NaOL as a function of pH.

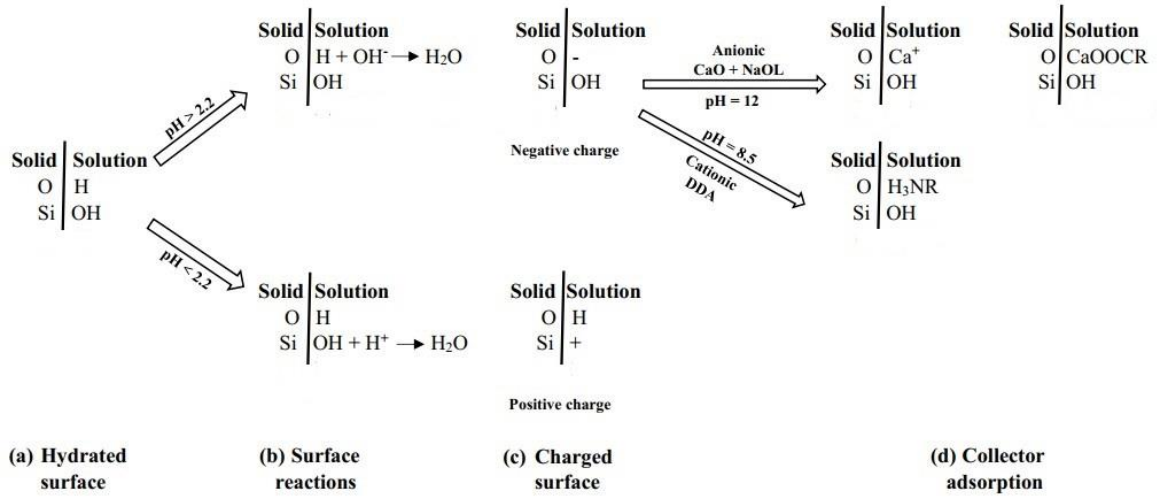

Fig. 7. Origin of charge on quartz: (a) depiction of hydrated Si and O sites, (b) reaction at low pH with H^+ and at high pH with OH^-, (c) the resulting positive and negative charged surface sites, and (d) adsorption of H_3NR^+ or $RCOOCa^+$ on negatively charged surface site.

Results and Discussion

Flotation experiment

The Half-Normal graph of the DDA collector in Fig. 8(a) shows that the most significant impacts were caused by fine particles (C), MIBC (A), and pulp concentration (B). Froth depth (D) had no substantial effect on the recovery. The use of NaOL as a collector resulted in calcium oxide (E), MIBC (A), and fine particles (C) having the most significant influence, as shown by the Half-Normal Plot in Fig. 8(b) (Abbaker & Nevzat, 2023). The froth depth plays a crucial role in the recovery process. By reducing the residence time, a decrease in froth depth enhances the recovery of larger particles, leading to a modest improvement in the total recovery rate. Nevertheless, this process would lead to concentrated contamination due to the increased retrieval of gangue by entrainment (Duffy et al., 2013; Rahman et al., 2012). Froth depth had little effect on the recovery of coarse particles relative to other influencing parameters in a 1.2 L flotation cell in both cationic and anionic collectors.

Perturbation plots were used to explain the independent variable's primary effects on recovery. The factor codes had the same meaning for both collector variables but only differed depending on the collector type, which was either DDA or NaOL. The perturbation plot in Fig. 9(a) displays the main effects of MIBC (A), pulp concentration (B), fine particles (C), impeller speed (D), and DDA (E) on the recovery when microbubbles were not present. Without microbubbles, the factors with the greatest influence on recovery are impeller speed (D), DDA (E), and particle concentration (C). On the other hand, MIBC (A) and pulp concentration (B) have little influence. When changing the environment from cationic to anionic, as in Fig. 9(b), NaOL (E) has the most significant effects on recovery subsequent to fine particles (C) and impeller speed (D). Moreover, pulp concentration (B), calcium oxide (F), and MIBC (A) have little to no impact on the response (Abbaker & Nevzat, 2023). It has been noticed that the overall value of the response of the cationic collector was higher than that of the anionic collector, and the factor's effects were more apparent. The adsorption mechanism of the collectors at different pH may be the reason for the result.

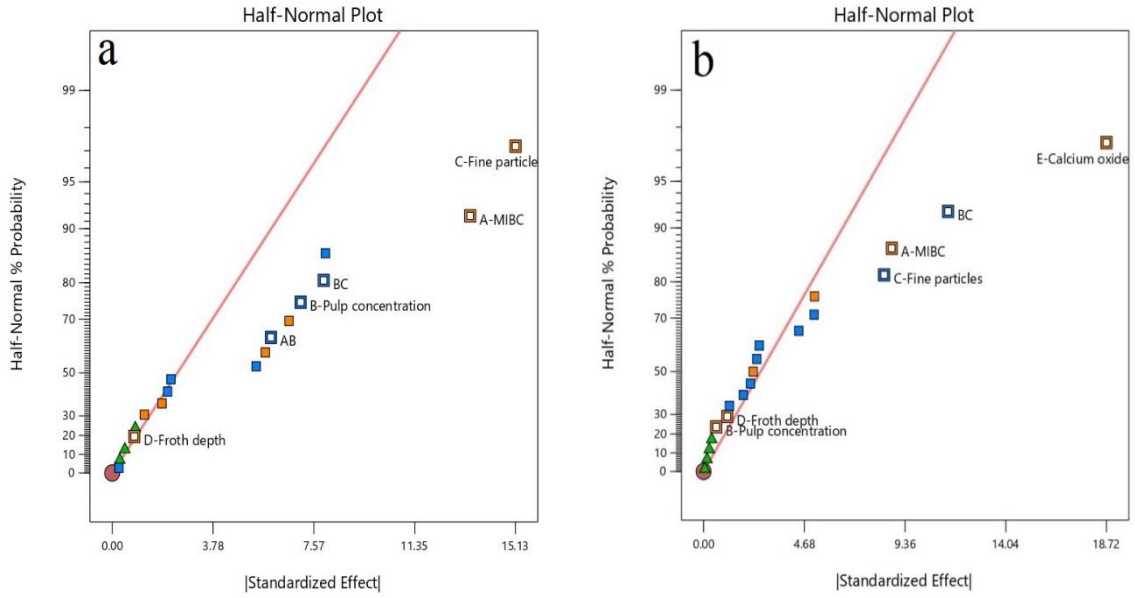

Fig. 8. Half-Normal Plots of the main effects of MIBC (A), Pulp concentration (B), Fine particles (C), Froth depth (D), and Calcium oxide (E) when using (a) DDA and (b) NaOL as a collector.

In the existence of microbubbles, the average recovery in the cationic environment increased by nearly 15%; otherwise, the effect characteristics of the variables have the same pattern as in the absence of microbubbles, as shown in perturbation plots in Fig. 10(a). However, the anionic conditions showed a different behavior when using microbubbles in Fig. 10(b). The recovery increased by more than 10%, and the most affected variables are NaOL (E) and impeller speed (D), followed by fine particles (C), calcium oxide (F), and pulp concentration (B), where MIBC (A) presents a slight impact on the recovery (Abbaker & Nevzat, 2023).

Using microbubbles has increased the average of overall recovery. This result can be explained by the fact that microbubbles increase the likelihood of the attachment of particle bubbles. This is due to the well-known "bridge effect" or "secondary collector role," in which many ultrafine bubbles combine with coarse bubbles on the surface of minerals (Nazari & Hassanzadeh, 2020). Because of the microbubbles' enormous surface area, which increases the likelihood of particle-bubble collision and adhesion, the total recovery improved in the presence of the hydrophobic particles (Li et al., 2020; Nazari et al., 2019; Tao, 2005).

The detachment of particles from bubbles rises when the surface hydrophobicity decreases, which occurs due to a decrease in the covering of collectors (Farrokhpay & Fornasiero, 2017); accordingly, when the collector quantity grows, so does the attachment, and the recovery rate increases more with the use of microbubbles. The use of surfactants is widely acknowledged to lower surface tension and bubble size and have an effect similar to that of a frother (Cho & Laskowski, 2002). However, the collector impacted the coarse particle flotation process more than the frother. The insertion of microbubbles helps to elucidate this effect. The hydrophobic particles and bubbles are effectively contacted and distributed uniformly by microbubbles. According to Nazari (2019), the collector's presence can compensate for the frother's absence in microbubble-assisted flotation (Nazari et al., 2019). Wiese (2010) found that the overuse of the frother may cause the froth to become unstable and have a poor recovery (Wiese et al., 2010). An excessively stable froth might hinder the entrapment of mineral particles in the concentrate, causing them to be directed towards the tailings.

At low impeller speeds, the probability of collusion diminishes due to the reduced force required to blend the dense particles. Consequently, these particles settle in the pulp, leading to suboptimal recovery (Nazari et al., 2018). Still, the probability of collision and detachment rises significantly with higher impeller speeds, and the flotation recovery is primarily contingent upon the adhesion between the particle and the bubble (Darabi et al., 2019). This relationship is finite because the particle-bubble aggregates created in the pulp will probably be demolished at impeller speeds exceeding 1300 rpm when severe hydrodynamic conditions predominate following a successful collision and attachment (Nazari et al., 2018; Shahbazi et al., 2009).

A specific quantity of fine quartz particles in the pulp enhanced large quartz particle's ability to float, which changed the appearance of the froth and caused the bubbles to become more stable and smaller—a process that is analogous to that of frothers (Ata & Jameson, 2013; Gupta et al., 2007; Vieira & Peres, 2007). The effects of fine particles in coarse particle flotation might differ based on factors such as flotation conditions, particle size distribution, and particle surface characteristics. By adjusting the flotation process parameters, the benefits of fine particles may be maximized, and the performance of coarse particle flotation can be improved.

Increased pulp density leads to greater probabilities of particle-bubble collisions, resulting in more mineral particles adhering to air bubbles and being transported to the froth phase (Duffy et al., 2013). Introducing

microbubbles enhances the effective capacity of the flotation pulp. The void proportion of the pulp rises due to its greater surface area compared to normal bubbles. Consequently, this effectively lowers the bulk density of the pulp, decreasing the pulp's overall density.

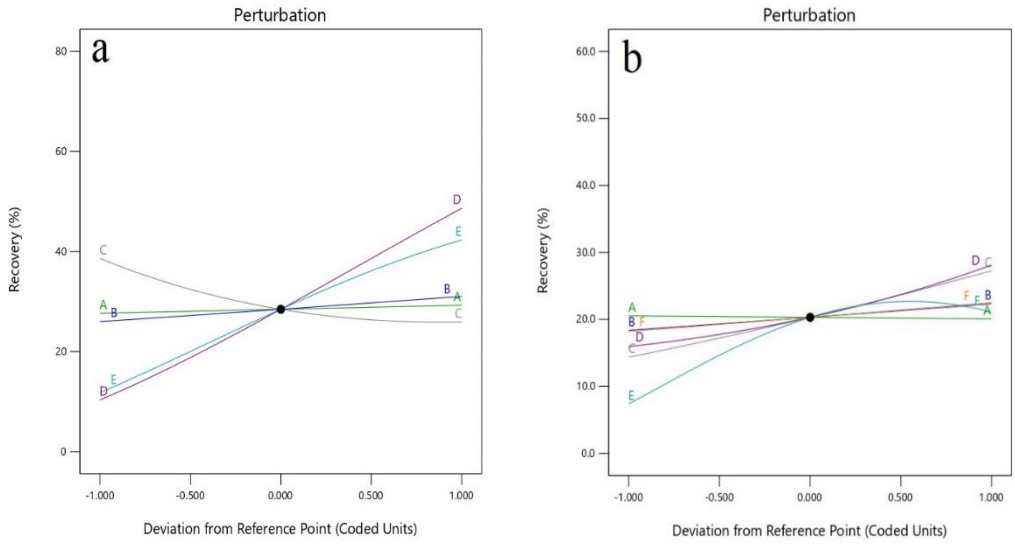

Fig. 9. Perturbation plots of recovery presenting the main effects of MIBC (A), pulp concentration (B), fine particles (C), impeller speed (D), DDA / NaOL (E), and calcium oxide (F) when using (a) cationic and (b) anionic as a collector in the absence of Microbubbles.

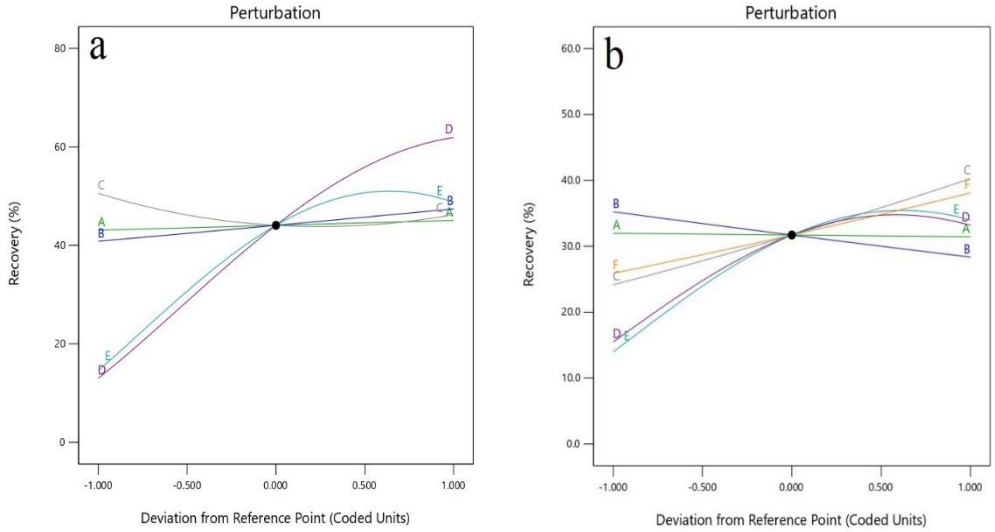

Fig. 10. Perturbation plots of recovery presenting the main impacts of MIBC (A), pulp concentration (B), fine particles (C), impeller speed (D), DDA / NaOL (E), and calcium oxide (F) when using (a) cationic and (b) anionic as a collector in the presence of Microbubbles.

Contact angle tests and EDX analysis

The contact angle is a valuable parameter for assessing the wetting properties of a solid surface. It may be used to determine the degree of hydrophobicity or hydrophilicity based on the contact angle measurement. Thus, the contact angles of mineral samples were determined under various situations, and the changes in the contact angles of quartz when using different concentrations of DDA, calcium oxide, and NaOL were presented. It was clear that with increasing collector concentrations, either cationic or anionic, the contact angle increases due to the adsorption of the collector in more areas of the quartz surface and increases the hydrophobicity. For comparison, in Figs. 11(a, b), the contact angles of DDA are generally higher than those of NaOL. This result explains why the cationic collector performed better than the anionic collector. The contact angles of the anionic collector proved that NaOL adsorption on the quartz surface depends totally on the activation of CaO.

The chemical analysis using EDX on the surface of quartz before and after treatment revealed that the elements of the collectors used had been recorded on the surface. Thus, Fig. 12 shows that the pure quartz elements were Si and O, whereas after being treated with DDA, the elements were Si, O, C, and N, as shown in Fig. 13. When CaO and NaOL were used, the elements were Si, O, C, Ca, and Na, as shown in Fig. 14. The existence of these elements on the surface of quartz proves that the collectors have been adsorbed successfully.

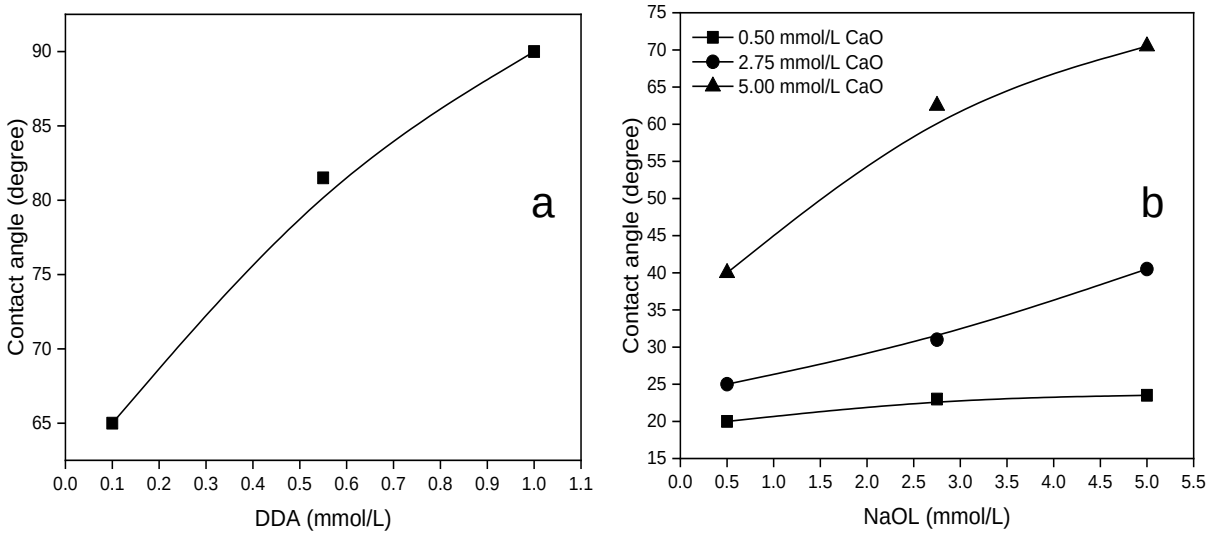

Fig. 11. The contact angle of quartz treated with a) DDA and b) NaOL at different CaO concentrations.

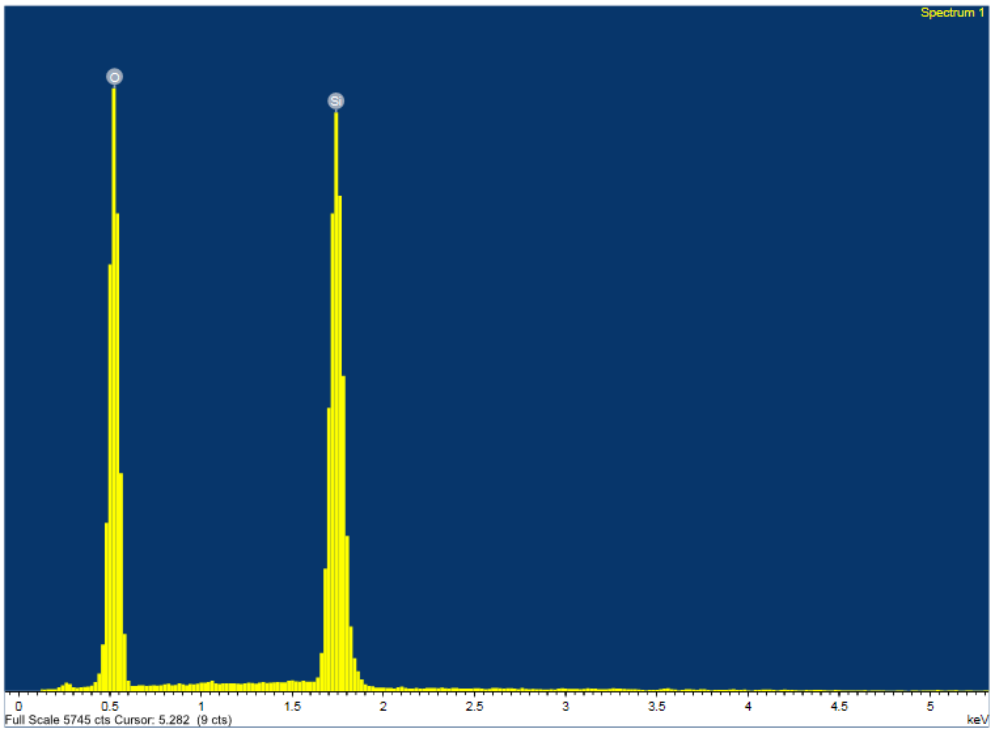

Fig. 12. EDX spectroscopy analysis of quartz.

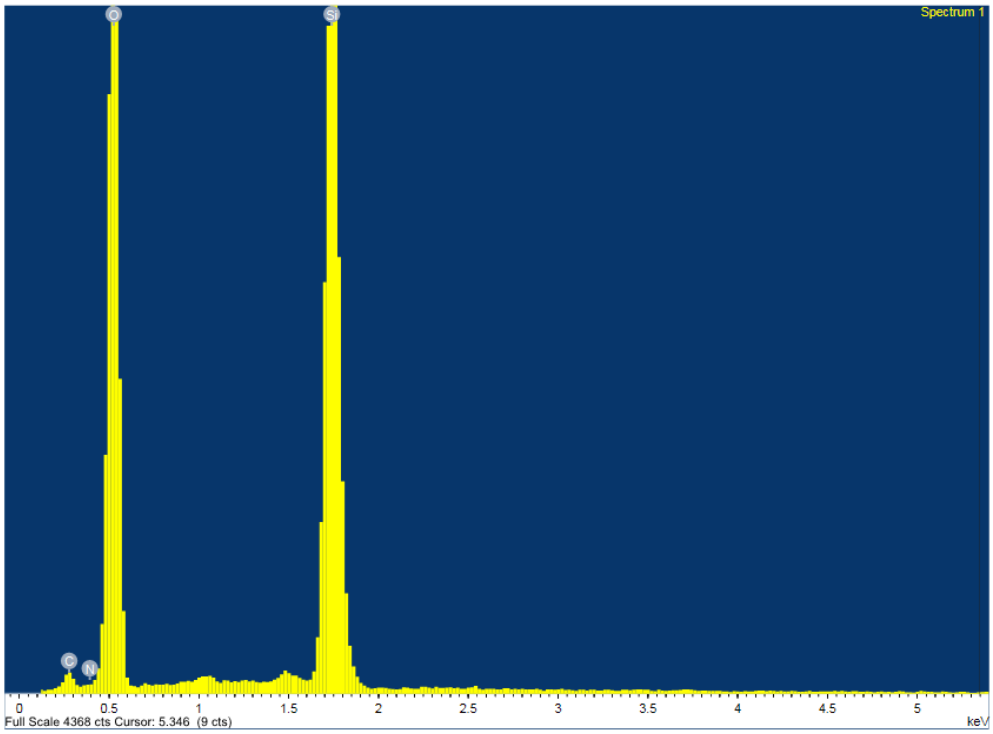

Fig. 13. EDX spectroscopy analysis of quartz treated with DDA.

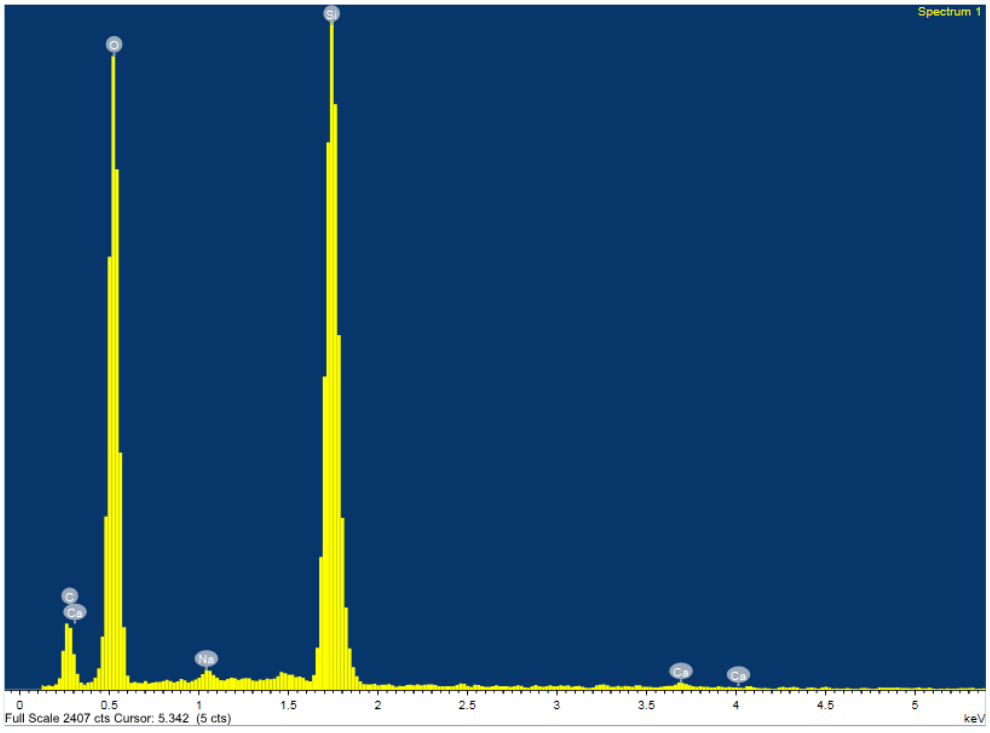

Fig. 14. EDX spectroscopy analysis of quartz treated with CaO and NaOL.

Adsorption Quantity

Accurate adsorption data is essential for a clean fitting procedure to study the DDA and NaOL adsorption behaviors. In both collector adsorption cases, it is apparent from Fig. 15(a, b) that the amount of collectors adsorbed increased with their concentrations. Despite DDA's lower concentration, it performed better than NaOL, and the adsorption amount was more effective. The reason for that is the adsorption mechanism of both collectors, wherein in the cationic collector, the RNH^{3+} is adsorbed directly to the quartz surface and is characterized by high selectivity. Still, in the anionic collector, the Ca^{+2} first activates the quartz surface by changing its charge from

negative to positive, allowing $RCOO^-$ to adsorb. It is clear from Fig. 21 that there was no adsorption of the anionic collector in the absence of the activator; hence, the adsorption of NaOL increased with an increase in CaO.

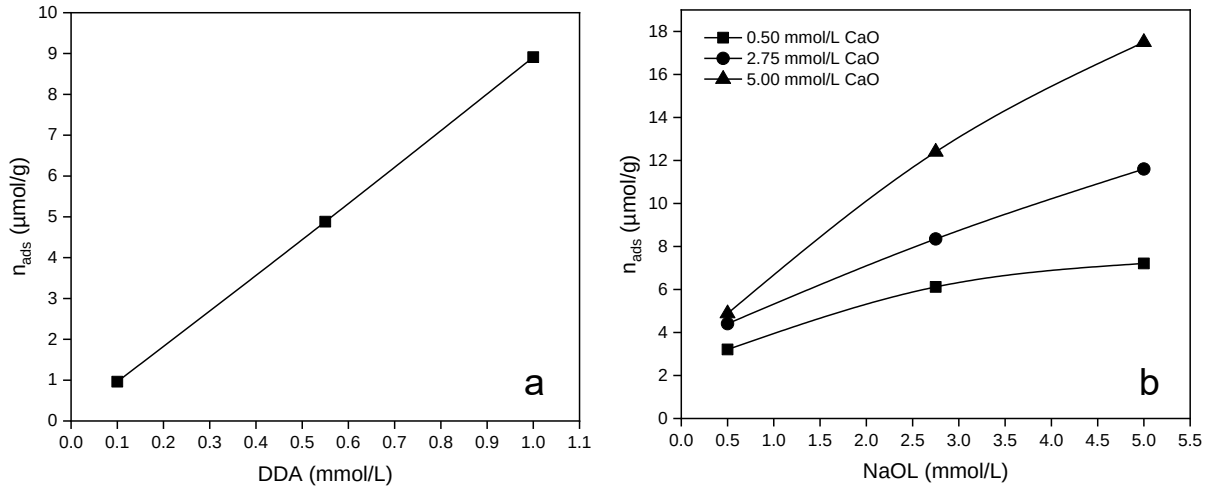

Fig. 15. Adsorption amount of a) DDA and b) NaOL at different CaO concentrations onto quartz.

Zeta potential

Zeta potential tests were carried out to investigate the reaction mechanism of DDA and NaOL on the quartz surface. The zeta potential of quartz was measured at a pH of 8.5 when treated with DDA and at a pH of 12 when treated with CaO and NaOL at different concentrations. The pure quartz without any treatment was measured at pH 8.5 and 12, resulting in a zeta potential of -43.3 mV and -39.8 mV, respectively. When the zeta potential has a value near zero, it is better for treated quartz. Without using any collector, the zeta potential characterizes the surface charge, which is essential for choosing a collector; the next step is that the collector adsorbs on the surface, decreasing the potential of the charge. This behavior explains why, with the increase in the collector concentration, the value of the zeta potential moves to zero, as shown in Fig. 16(a, b). As the results present, the NaOL could get the same results as DDA if it has enough CaO and its concentration is almost five times higher than that of DDA concentration.

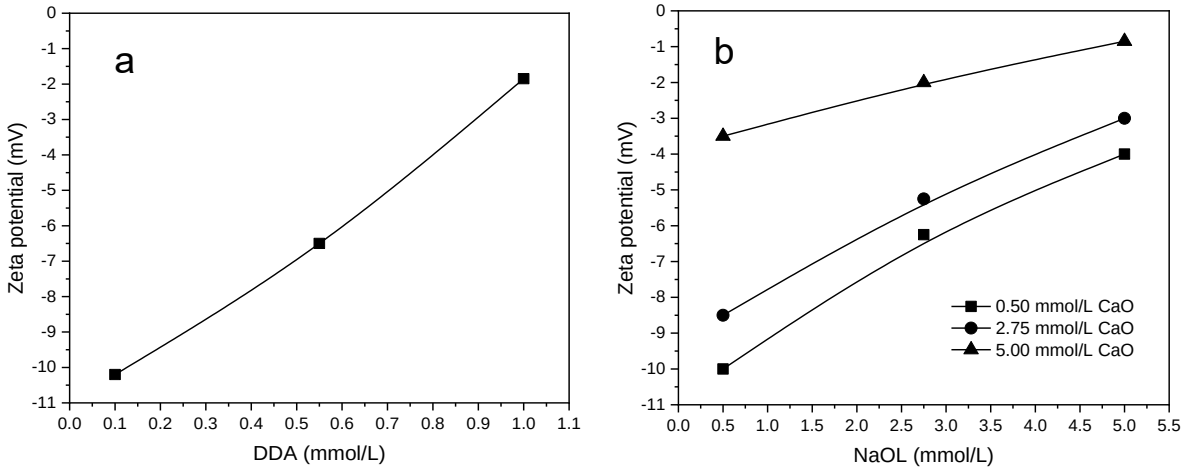

Fig. 16. Zeta potential of quartz treated with a) DDA and b) NaOL at different CaO concentrations.

FT-IR spectra

Structures are frequently identified using infrared spectroscopy because functional groups produce distinctive bands distinct in intensity and position (frequency). It has been demonstrated that FT-IR spectroscopy analysis is a valuable technique for identifying the adsorption models on minerals. This case was carried out to learn more about the adsorption process between DDA and NaOL. The functional groups of the quartz, DDA, CaO, and NaOL before and following treatment have been examined and determined; Figs. 17 and 18 display the FT-IR spectra of these samples.

The stretching vibrations of the silicon-oxygen tetrahedron groups are represented by the peaks at 1858 cm^{-1} in the quartz spectrum curve. The Si-O groups' bending vibration is responsible for the prominent peaks at 1035

cm^{-1}. Furthermore, the stretching vibrations of the Si-O-Si groups were identified as the cause of the peaks at 692 and 776 cm^{-1} (Liu et al., 2020) The peaks in the infrared spectra of NaOL were identified as the typical absorption peak of carboxyl groups in the material at about 1559 cm^{-1}, and the peaks at around 2850 and 2920 cm^{-1} were ascribed to the asymmetric and symmetric stretching of -CH_2- and -CH_3 (Zhu et al., 2018). The O-H bond is responsible for the peak at 3642 cm^{-1} in the CaO spectrum, whereas the stretching vibration of the Ca-O bond is responsible for the peaks at 1418 and 874 cm^{-1}. In the DDA spectra, the bonds at 1667 and 653.83 cm^{-1} are attributable to the N–H bending vibration, while a large peak at 3331 cm^{-1} is associated with the N–H stretching vibrations. Furthermore, the bending vibrations of the -CH_3 and -CH_2- groups were identified as the source of the peaks at 2917 and 2849 cm^{-1}, whereas the stretching vibrations of the C–N groups are represented by the peaks at 1257 and 921 cm^{-1} (Liu et al., 2020).

The bond strength of the stretching vibrations of the N-H groups at 1685 cm^{-1} has been detected in the quartz spectra following treatment with DDA. This result indicates that DDA has been adsorbed on the quartz surface. On the other hand, the sample treated with CaO and NaOL showed stretching vibrations at 2920 and 2851 cm^{-1}, which resulted from the -CH_2- and -CH_3 groups, and at 1561 cm^{-1} from the carboxyl groups, both of which belong to NaOL. The results of FT-IR present different groups of elements that were adsorbed on a quartz surface when using DDA and NaOL. However, both collectors were chemically adsorbed.

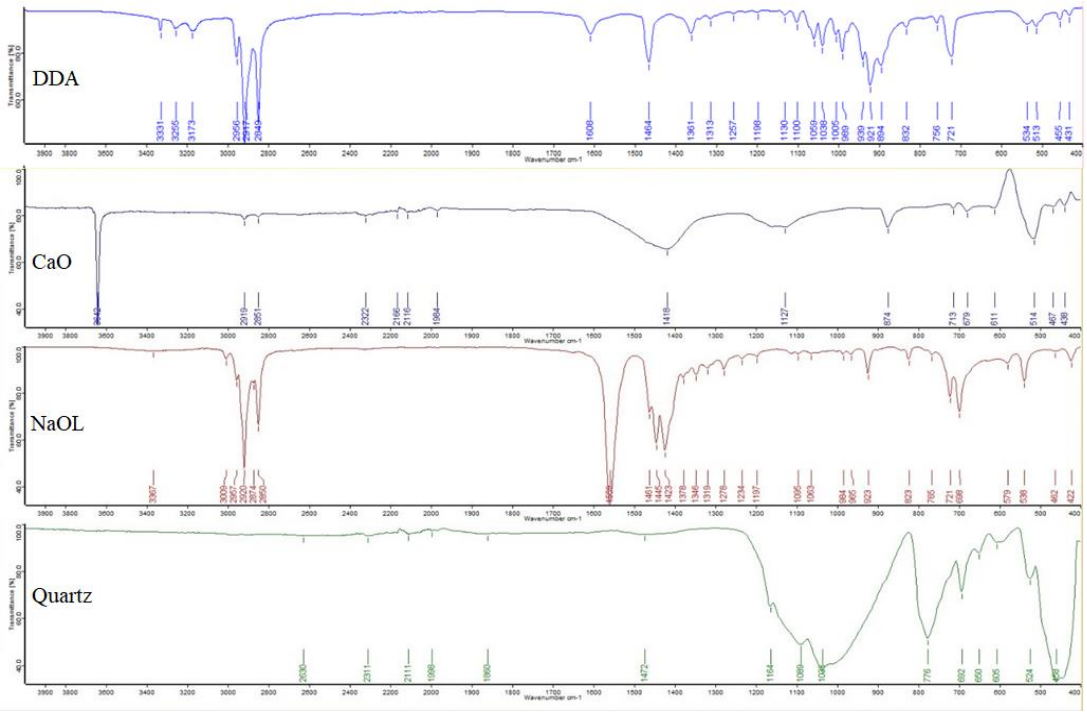

Fig. 17. FT-IR spectrum of DDA, CaO, NaOL, and quartz.

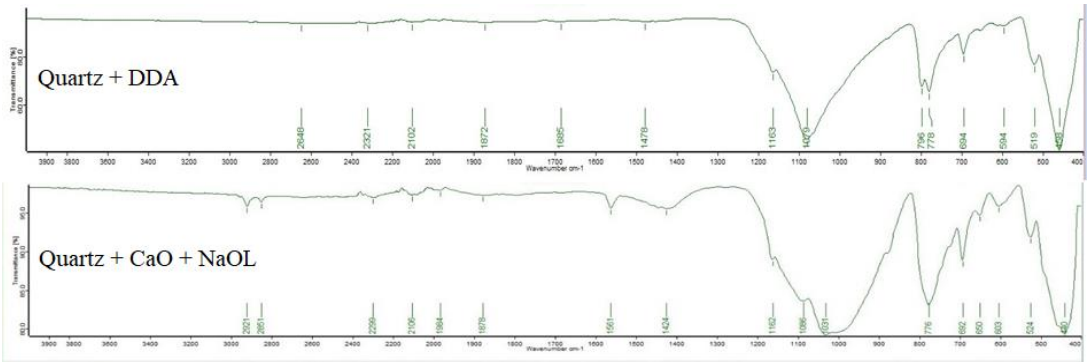

Fig. 18. FT-IR spectrum of quartz treated with 1 x 10^{-3} mol/L of DDA and 5 x 10^{-3} mol/L of both CaO + NaOL.

Conclusions

Coarse particle flotation has several advantages, including decreased filtering, thickening, drying expenses, and enhanced plant throughput. This study compares the performance and adsorption characteristics for coarse quartz particle microbubble-assisted flotation using a two-factorial level and Box-Behnken analysis design. When NaOL and DDA were used, the froth depth had no major impact on the flotation process. The average recovery of the cationic collector at the mean values of the parameters was >10% greater than that of the anionic collector, in which DDA outperforms NaOL in both the presence and absence of microbubbles. In the anionic environment, the flotation parameters behaved somewhat differently when employing microbubbles, but in the cationic conditions, a distinct pattern was presented with and without microbubbles. According to the contact angle study, utilizing NaOL under optimal conditions was measured around 70°, whereas DDA was approximately 90°. DDA has been adsorbed more on the quartz surfaces than NaOL at the same collector concentration. Furthermore, the negative zeta potential of quartz in an alkaline pH environment increased with increasing concentrations of both collectors, where zeta potential shows greater sensitivity for DDA. DDA and NaOL were chemically adsorbed onto quartz surfaces, as FT-IR and EDX data demonstrated. Finally, the investigation demonstrates that DDA outperformed NaOL in the flotation of coarse quartz particles, whether microbubbles were present or absent.

References

Abbaker, A., Nevzat, A. (2023) The effect of microbubbles on coarse particle anionic flotation: analysis and optimization. *Physicochemical Problems of Mineral Processing*, 59, 172298. https://doi.org/10.37190/ppmp/172298

Ata, S., Jameson, G.J. (2013b) Recovery of coarse particles in the froth phase–A case study. *Minerals Engineering*, 45, 121–127. https://doi.org/10.1016/j.mineng.2013.02.006

Cao, S., Yin, W., Yang, B., Zhu, Z., Sun, H., Sheng, Q., Chen, K. (2022) Insights into the influence of temperature on the adsorption behavior of sodium oleate and its response to flotation of quartz. *International Journal of Mining Science and Technology*, 32, 399–409. https://doi.org/10.1016/j.ijmst.2021.12.006

Carlos de F. Gontijo, Daniel Fornasiero, John Ralston (2007) 740 the Canadian Journal of Chemical Engineering.

Cho, Y.S., Laskowski, J.S. (2002) Effect of flotation frothers on bubble size and foam stability, *International Journal of Mineral Processing*. 64(2-3), 69-80. https://doi.org/10.1016/S0301-7516(01)00064-3

Darabi, H., Koleini, S.M.J., Deglon, D., Rezai, B., Abdollahy, M. (2019) Investigation of bubble-particle interactions in a mechanical flotation cell, part 1: Collision frequencies and efficiencies. *Minerals Engineering*. 134, 54–64. https://doi.org/10.1016/j.mineng.2019.01.012

Duffy, K.-A., Runge, K., Tabosa, E. (2013). Strategies for increasing coarse particle flotation in conventional flotation cells. Proc. the 6th Int. Flotation Conf.

Elvers, B. (1991) Ullmann's encyclopedia of industrial chemistry. Verlag Chemie Hoboken, NJ.

Fan, G., Wang, L., Cao, Y., Li, C. (2020) Collecting agent–mineral interactions in the reverse flotation of iron ore: A brief review. *Minerals* 10, 681. https://doi.org/10.3390/min10080681

Farrokhpay, S., Ametov, I., Grano, S. (2011) Improving the recovery of low grade coarse composite particles in porphyry copper ores. In: *Advanced Powder Technology*. pp. 464–470. https://doi.org/10.1016/j.apt.2011.04.003

Farrokhpay, S., Filippov, L., Fornasiero, D. (2021) Flotation of fine particles: A review. *Mineral Processing and Extractive Metallurgy Review*. 42, 473–483. https://doi.org/10.1080/08827508.2020.1793140

Farrokhpay, S., Filippova, I., Filippov, L., Picarra, A., Rulyov, N., Fornasiero, D. (2020) Flotation of fine particles in the presence of combined microbubbles and conventional bubbles. *Minerals Engineering*. 155, 106439. https://doi.org/10.1016/j.mineng.2020.106439

Farrokhpay, S., Fornasiero, D. (2017) Flotation of coarse composite particles: Effect of mineral liberation and phase distribution. *Advanced Powder Technology*. 28, 1849–1854. https://doi.org/10.1016/j.apt.2017.03.012

Fosu, S., Skinner, W., Zanin, M. (2015) Detachment of coarse composite sphalerite particles from bubbles in flotation: Influence of xanthate collector type and concentration. *Minerals Engineering*. 71, 73–84. https://doi.org/10.1016/j.mineng.2014.10.014

Fu, X., Gao, Y., Han, H., Gao, Z., Wang, L., Sun, W., Yue, T. (2022) Quantization of the hydration and dodecylamine adsorption characteristics of hematite and quartz surface active sites to forecast the flotation behavior of minerals. *Minerals Engineering*. 183. https://doi.org/10.1016/j.mineng.2022.107571

Girgin, E.H., Do, S., Gomez, C.O., Finch, J.A. (2006) Bubble size as a function of impeller speed in a self-aeration laboratory flotation cell. *Minerals Engineering*. 19, 201–203. https://doi.org/10.1016/j.mineng.2005.09.002

Gupta, A.K., Banerjee, P.K., Mishra, A. (2007) Effect of frothers on foamability, foam stability, and bubble size. *Coal Preparation*. 27, 107–125. https://doi.org/10.1080/07349340701249794

Hassanzadeh, A., Safari, M., Hoang, D.H., Khoshdast, H., Albijanic, B., Kowalczuk, P.B. (2022) Technological assessments on recent developments in fine and coarse particle flotation systems. *Minerals Engineering*. 180:107509. https://doi.org/10.1016/j.mineng.2022.107509

Jameson, G.J. (2010) Advances in fine and coarse particle flotation. In: *Canadian Metallurgical Quarterly*. 49.4 (2010): 325-330. https://doi.org/10.1179/cmq.2010.49.4.325

Kromah, V., Powoe, S.B., Khosravi, R., Neisiani, A.A., Chelgani, S.C. (2022) Coarse particle separation by fluidized-bed flotation: A comprehensive review. *Powder Technology*. 409, 117831. https://doi.org/10.1016/j.powtec.2022.117831

Li, Y., Wu, F., Xia, W., Mao, Y., Peng, Y., Xie, G. (2020) The bridging action of microbubbles in particle-bubble adhesion. *Powder Technology*. 375, 271–274. https://doi.org/10.1016/j.powtec.2020.07.109

Liu, A., Fan, P.P., Qiao, X.X., Li, Z.H., Wang, H.F., Fan, M.Q. (2020) Synergistic effect of mixed DDA/surfactants collectors on flotation of quartz. *Minerals Engineering*. 159. https://doi.org/10.1016/j.mineng.2020.106605

Nazari, S., Chehreh Chelgani, S., Shafaei, S.Z., Shahbazi, B., Matin, S.S., Gharabaghi, M. (2019) Flotation of coarse particles by hydrodynamic cavitation generated in the presence of conventional reagents. *Separation and Purification Technology*. 220, 61–68. https://doi.org/10.1016/j.seppur.2019.03.033

Nazari, S., Hassanzadeh, A. (2020) The effect of reagent type on generating bulk sub-micron (nano) bubbles and flotation kinetics of coarse-sized quartz particles. *Powder Technology*. 374, 160–171. https://doi.org/10.1016/j.powtec.2020.07.049

Nazari, S., Hassanzadeh, A., He, Y., Khoshdast, H., Kowalczuk, P.B. (2022) Recent Developments in Generation, Detection and Application of Nanobubbles in Flotation. *Minerals*. 2(4), 462. https://doi.org/10.3390/min12040462

Nazari, S, Shafaei, S.Z., Gharabaghi, M., Ahmadi, R., Shahbazi, B. (2018) Effect of frother type and operational parameters on nano bubble flotation of quartz coarse particles. *Journal of Mining & Environment*. 9, 539–546. https://doi.org/10.22044/jme.2017.6404.1461

Nazari, Sabereh, Shafaei, S.Z., Gharabaghi, M., Ahmadi, R., Shahbazi, B., Maoming, F. (2019) Effects of nanobubble and hydrodynamic parameters on coarse quartz flotation. *International Journal of Mining Science and Technology*. 29, 289–295. https://doi.org/10.1016/j.ijmst.2018.08.011

Nazari, S., Shafaei, S.Z., Shahbazi, B., Chehreh Chelgani, S. (2018) Study relationships between flotation variables and recovery of coarse particles in the absence and presence of nanobubble. *Colloids and Surfaces A: Physicochemical and Engineering Aspects*. 559, 284–288. https://doi.org/10.1016/j.colsurfa.2018.09.066

Rahman, R.M., Ata, S., Jameson, G.J. (2012) The effect of flotation variables on the recovery of different particle size fractions in the froth and the pulp. *International Journal of Mineral Processing*. 106–109, 70–77. https://doi.org/10.1016/j.minpro.2012.03.001

Rao, S.R. (2013) Surface chemistry of froth flotation: Volume 1: Fundamentals. Springer Science & Business Media.

Rulyov, N., Nessipbay, T., Dulatbek, T., Larissa, S., Zhamikhan, K. (2018) Effect of microbubbles as flotation carriers on fine sulphide ore beneficiation. *Mineral Processing and Extractive Metallurgy*. 127, 133–139. https://doi.org/10.1080/03719553.2017.1351067

Rulyov, N.N., Sadovskiy, D.Y., Rulyova, N.A., Filippov, L.O. (2021) Column flotation of fine glass beads enhanced by their prior heteroaggregation with microbubbles. *Colloids and Surfaces A: Physicochemical and Engineering Aspects*. 617, 126398. https://doi.org/10.1016/j.colsurfa.2021.126398

Shahbazi, B., Rezai, B., Koleini, S.M.J. (2009) The effect of hydrodynamic parameters on probability of bubble–particle collision and attachment. *Minerals Engineering*. 22, 57–63. https://doi.org/10.1016/j.mineng.2008.03.013

Tao, D. (2005) Role of Bubble Size in Flotation of Coarse and Fine Particles - A Review. Separation science and technology. 39.4. 741-760. https://doi.org/10.1081/SS-120028444

Tussupbayev, N.K., Rulyov, N.N., Kravtchenco, O. V. (2016) Microbubble augmented flotation of ultrafine chalcopyrite from quartz mixtures. *Mineral Processing and Extractive Metallurgy*. 125, 5–9. https://doi.org/10.1179/1743285515Y.0000000014

Vieira, A.M., Peres, A.E.C. (2007) The effect of amine type, pH, and size range in the flotation of quartz. *Minerals Engineering*. 20, 1008–1013. https://doi.org/10.1016/j.mineng.2007.03.013

Wiese, J.G., Harris, P.J., Bradshaw, D.J. (2010) The effect of increased frother dosage on froth stability at high depressant dosages. In: *Minerals Engineering*. 23(11-13), 1010-1017. https://doi.org/10.1016/j.mineng.2010.04.011

Xu, D., Ametov, I., Grano, S.R. (2011) Detachment of coarse particles from oscillating bubbles—The effect of particle contact angle, shape and medium viscosity. *International Journal of Mineral Processing*. 101, 50–57. https://doi.org/10.1016/j.minpro.2011.07.003

Zhu, H., Valdivieso, A.L., Zhu, J., Min, F., Song, S., Huang, D., Shao, S. (2018) Effect of dodecylamine-frother blend on bubble rising characteristics. *Powder Technology*. 338, 586–590. https://doi.org/10.1016/j.powtec.2018.07.031